Published by SET Publisher

Journal of Basic & Applied Sciences

ISSN (online): 1927-5129

Structural and Dielectric Properties of Ba-Doped BNT Ceramics

Khushboo Thapa[1], Priyanka Thankur[1], Navdeep Sharma[2], Sanjeev Sharma[3], Asad Ali[4], Abid Zaman[5] and Madan Lal[1,*]

[1]*Department of Physics, ACBS, Eternal University, Sirmour, HP 173101, India*

[2]*Department of Physics & Astronomical Sciences, Central University of Jammu, J&k 181143, India*

[3]*Department of Chemistry, School of Applied Sciences, Om Sterling Global University, Hisar 125001, India*

[4]*Department of Physics, Post Graduate College Nowshera, 24100, Pakistan*

[5]*Department of Physics, Riphah International University Islamabad, 44000, Pakistan*

Article Info:

Keywords:
X-ray diffraction,
BNT,
Ceramics,
Dielectric,
Ac-conductivity.

Timeline:
Received: January 29, 2022
Accepted: February 15, 2022
Published: April 05, 2022

Citation: Thapa K, Thankur P, Sharma N, Sharma S, Ali A, Zaman A, Lal M. Structural and Dielectric Properties of Ba-Doped BNT Ceramics. J Basic Appl Sci 2021; 18: 47-57.

DOI: https://doi.org/10.29169/1927-5129.2022.18.06

Abstract:

In this study, lead-free Ba-doped $((Bi_{(0.5)}Na_{0.5})TiO_3$ ceramics were synthesized by the conventional solid-state reaction method and characterized by X-ray diffraction technique, which indicates the pure crystalline nature of ceramics with ABO_3 symmetry. The splitting in the peaks reveals that the ceramics with x = 0.10 and 0.30 are well in Morphotrophic Phase Boundary where rhombohedral and tetragonal phases co-exist. The scanning electron microscope images show that the average grain size of the ceramics increases with an increase in the Ba concentration. Dielectric properties of pure and Ba-doped $((Bi_{(0.5)}Na_{0.5})TiO_3$ceramics measured by LCR meter in the frequency range of 1 k Hz – 1 M Hz shows the decrease in the value of dielectric constant with an increase in frequency. ε_{max} = 5563 was obtained at x = 0.30 with T_C = 300 °C at the frequency of 1 k Hz, whereas σ (f) curves were found to be merging at a high value of frequency and temperature regions.

*Corresponding Author
E-mail: madan.physics26@gmail.com

1. INTRODUCTION

In the 20th century, Pb-based ceramics have ruled the industries in the field of piezoelectric actuators, sensors, and transducers owing to their excellent piezoelectric, and ferroelectric properties. But up to the end of the 20th century, Pb imposes strong threats to the environment and human life. Therefore, there is a need to develop lead-free ceramics having high piezoelectric properties as those responses lead-based possess significant economic and social values. So, over the numerous experiments, scientists ables to find several alternatives (i.e. lead-free piezoelectric ceramics) to Pb like $(Bi_{0.5}Na_{0.5})TiO_3$ **(**BNT), $(Bi_{0.5}K_{0.5})TiO_3$ **(**BKT), $(Ki_{0.5}Na_{0.5})NbO_3$ (KNN), etc [1, 2].

Ferroelectric Bismuth sodium titanate (BNT) was discovered by Smolenski *et al.* [3] in 1959 and has been most extensively studied. Ferroelectric materials of the perovskite family (i.e. ABO_3-type) have received great attention from the last few decades due to their promising potential for various device applications like piezoelectric transducers, pyroelectric sensors/ detectors, electrostrictive actuators, multilayer capacitors (MLCCs), etc [4-6]. BNT ceramics have unique superiority because Bi^{3+} has a similar electronic structure (long pairs $6s^2$ electrons) with Pb^{2+}. This $6s^2$ pair of electrons leads to the high polarizable nature of BNT, which makes it potential application in actuators [7, 8].

BNT is also an A-site complex perovskite ferroelectric relaxor material and is recognized due to its high Curie temperature T_C = 320 °C. Pure BNT ceramics has a large coercive field E_C = 73 kV cm^{-1} at room temperature as well as a phase transition from rhombohedral to tetragonal below Curie temperature [9]. A lot of BNT based ceramics have been reported for their high-temperature dielectric behavior [10-12]. As BNT contains Bi, Na ions, these are highly volatile at higher temperatures and most difficult to pole due to their high ion conductivity. High conductivity is due small loss of Bi_2O_3 amount during the ceramics synthesis and processing of BNT ceramics at high temperatures [13-15]. This problem was later overcome by using 10-15% excess amount of Bi_2O_3 and Na_2CO_3 during its processing. But an extremely small amount of oxygen vacancy (i.e. about 0.005~0.0025) were resulting in high oxide conductivity which implies that the mobility of oxygen ions in BNT is very high [16]. The structural, dielectric, and electrical properties of BNT ceramics have been improved and enhanced by the substitution of dopants on A and B-site cations, such as Li, Al, La, Ta, Nb, Mg, Zr, Hf, etc [17-20]. In 1993, Takenaka *et al.* [21] reported that BNBT6 ceramics with MPB (Morphotrophic Phase Boundary), have relatively good piezoelectric properties [22]. Ba doped BNT also shows MPB with x = 0.10 as reported by Yadav [23] with relaxor-like behavior.

Pure BNT ceramics are restricted to various applications due to some of their shortcomings in properties like low dielectric constant, exhibiting weak piezoelectricity high conductivity at room temperature, and having a narrow sintering temperature range. These ceramics are also difficult to pole and sinter [23-25]. Therefore, to overcome these problems, Ba is doped on A-site in BNT and a modified solid-state method is used to synthesize BNT ceramics (i.e. used hot distilled water in place of ethanol) with the existence of MPB. In this report, we have synthesized pure and Ba-doped BNT ceramics using the conventional solid-state reaction method. Investigated their structure via X-ray diffraction (XRD), scanning electron microscope, and dielectric properties by an LCR meter.

2. MATERIALS AND METHODS

2.1. Raw Materials

The metal oxide and carbonates (high purity > 99%, Sigma Aldrich, India) Bismuth Oxide (Bi_2O_3), Sodium Carbonate (Na_2CO_3), Titanium Dioxide (TiO_2), Barium Carbonate ($BaCO_3$) were used as raw materials.

2.2. Experimental Procedure

The pure and Ba-doped $(Bi_{0.5}Na_{0.5})TiO_3$ ceramics were prepared by conventional solid-state reaction. These raw materials were weighed according to their stoichiometric ratio (as given in Table **1**) and milled continuously using an agate mortar and pestle in the hot distilled water medium for 10-12 h. Then calcined at 900 °C for 5hrs. The calcined powder was grinded and converted into green pellets (having 10 mm diameter and 2 mm thickness) by a hydraulic press under a pressure of 70 MPa (using 10% PVA solution as the binder). These green pellets were finally sintered in an alumina crucible containing Na_2CO_3, Bi_2CO_3 powders to suppress the volatility of Na, Bi at 1100 °C for 3 hrs.

2.3. Measurements

The X-ray diffraction (XRD) pattern of these ceramic composites was done using an X-ray diffractometer (Rigaku Miniflex II Desktop, Japan) in the 2θ range 20°

Table 1: Mass Percentage of Raw Materials Used for $((Bi_{(0.5-x)}Ba_x)Na_{0.5})TiO_3$ Ceramics

Composition (*x*)	Bi_2O_3	$BaCO_3$	Na_2CO_3	TiO_2	Total
0.00	52.274 %	--------	11.890 %	35.836 %	100
0.10	42.888 %	08.162 %	12.195 %	36.755 %	100
0.30	21.962 %	27.904 %	12.490 %	37.644 %	100

to 60°(with step size Δ2θ = 0.02°). Surface morphology was measured by Scanning electron microscopy (SEM) JEOL (JAPAN) JSM 6100. The polished surfaces of the sintered samples were electrodes with air-drying silver paste. Dielectric properties were done by using an LCR meter from 1 kHz to 1 MHz at different temperatures (RT-400 °C)

3. RESULTS AND DISCUSSION

3.1. X-Ray Diffraction (XRD)

Figure **1** shows the X-ray diffraction (XRD) patterns of $((Bi_{(0.5-x)}Ba_x)Na_{0.5})TiO_3$ (abbreviated as BBNT) with an increase in Ba content at room temperature. However, the spectrum of BBNT ceramics exhibits well-defined diffraction peaks at 2θ of 22.90, 32.62, 40.20, 46.75, 52.70 and 58.21 corresponding to (100), (110), (111), (200), (210) and (211) planes [26, 27]. It also confirmed that BNT at x = 0.00 has a rhombohedral structure with the space group R3c. With an increase of Ba^{2+} content, the diffraction peak shifts towards the lower angle 2θ. This peak shift indicates the increase in the volume of the unit cell because of the replacement of smaller ionic radii of Bi^{3+} (~1.17 Å) with larger ionic radii Ba^{2+} (1.39 Å). Also, the Ba^{2+} substituted BNT x = 0.30 shows the peaks (002) and (200) are merging into a single peak as shown in Figure **1b**. This may be due to the equal contribution of phases at this composition.

Rietveld refinement of the XRD pattern was done to further confirm the crystal structure and the lattice parameters (as shown in Figure **2**). Rietveld refinement also confirms that BBNT with x = 0.00 has rhombohedral, whereas BBNT for $x \geq 0.10$ exhibits the morphotropic phase boundary (MPB) where the rhombohedral and tetragonal structure co-exists [28]. The various Rietveld refined parameters are listed in Table **2**. The single-phase nature of BBNT ceramics is evident without a trace of any impurity phase. Thus, the sharp and clear peaks strongly confirm the pure crystalline nature of ceramics.

Figure **3** shows the fitting of the XRD peaks for (200), (210), and (211) planes of $((Bi_{(0.4)}Ba_{0.10})\ Na_{0.5})TiO_3$ ceramic fitted to the Gauss function. The coefficient R^2, interpreted as the best fit of a regression, determines the fitting of the peaks to the Gaussian function, which is closer to unity than other functions. But when R^2, is close to unity then the regression line fits the data well but if, close to zero then it is called a poor fit [29]. The

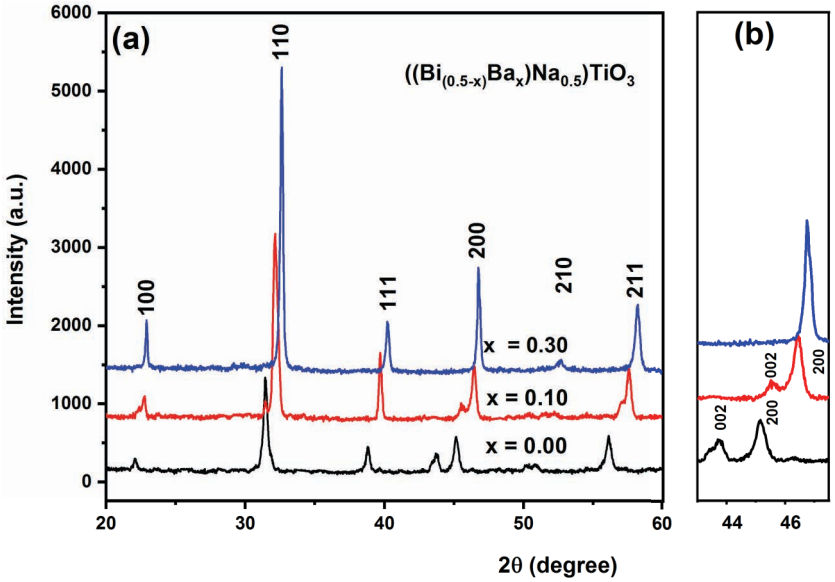

Figure 1: (**a**) XRD pattern of $((Bi_{(0.5-x)}Ba_x)Na_{0.5})TiO_3$ (where $0.00 \leq x \leq 0.30$) ceramics and (**b**) the enlarged view of (200) peak.

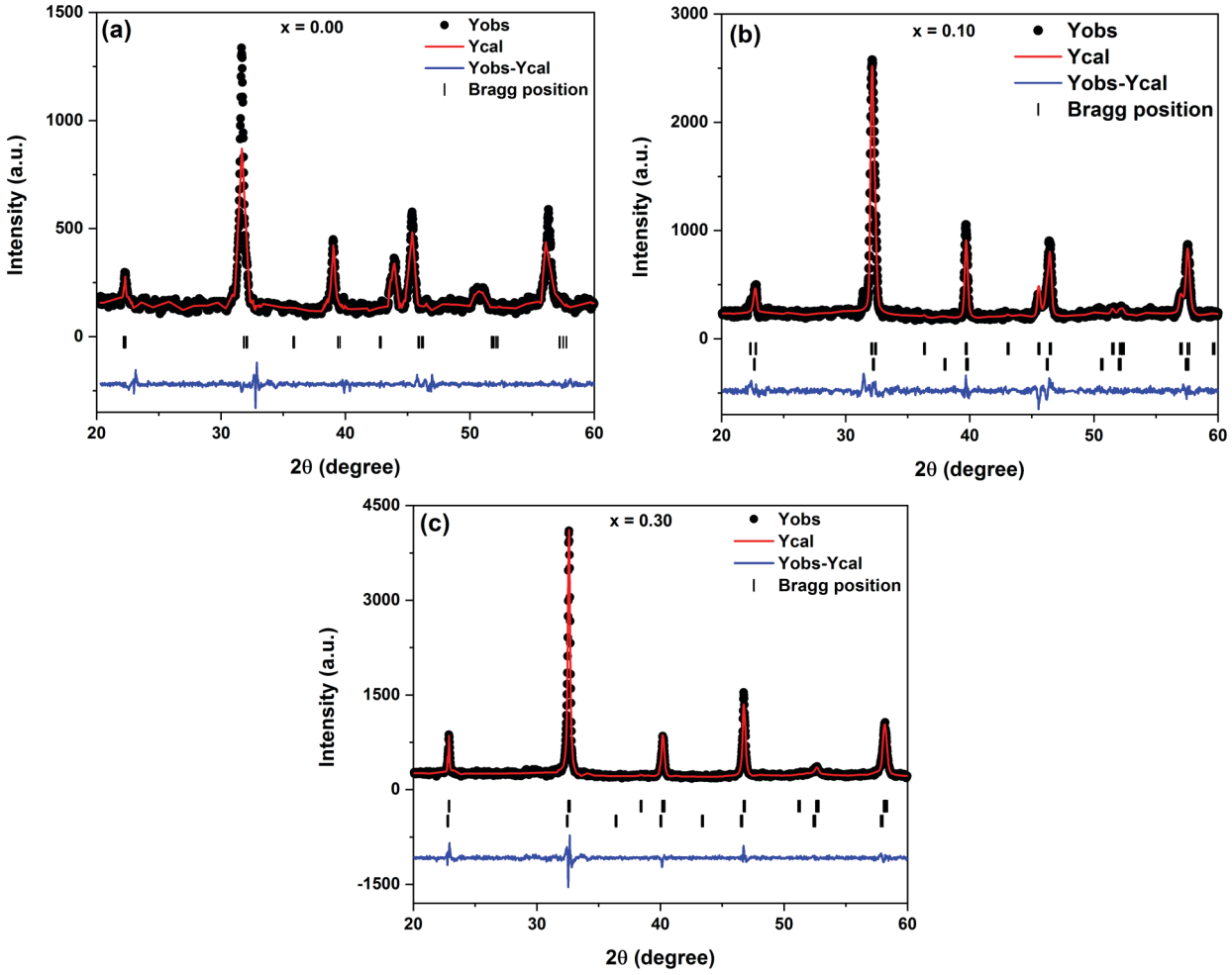

Figure 2: (**a-c**) Rietveld refinement of $((Bi_{(0.5-x)}Ba_x)Na_{0.5})TiO_3$ for x = 0.00, 0.10, and 0.30 ceramics.

Table 2: FullPROF Based Rietveld Refined Lattice Parameters and Atomic Positions of $((Bi_{(0.5-x)}Ba_x)Na_{0.5})TiO_3$ Ceramics

			x = 0.00	x = 0.10		x = 0.30	
Space group			**R3*c***	**R3*c***	**P4*bm***	**R3*c***	**P4*bm***
Lattice parameters	a = b (Å)		5.48870	5.49830	5.52660	5.49830	5.52660
	c (Å)		13.50480	13.43430	3.98200	13.43430	3.98200
Atomic positions		Bi	0.00000	0.00000	0.00000	0.00000	0.00000
	X	Ba	---------	0.00000	0.00000	0.00000	0.00000
		Na	0.00000	0.00000	0.00000	0.00000	0.00000
		Ti	0.00000	0.00000	0.00000	0.00000	0.00000
		O	0.12600	0.14283	0.27375	0.14283	0.27375
		Bi	0.00000	0.00000	0.50000	0.00000	0.50000
	Y	Ba	---------	0.00000	0.50000	0.00000	0.50000
		Na	0.00000	0.00000	0.00000	0.00000	0.00000
		Ti	0.00000	0.00000	0.00000	0.00000	0.00000
		O	0.33600	0.33691	0.22625	0.33691	0.22625
		Bi	0.26270	0.26227	0.52106	0.26227	0.52106
	Z	Ba	---------	0.26227	0.52106	0.26227	0.52106
		Na	0.26270	0.26227	0.52106	0.26227	0.52106
		Ti	0.00630	0.01411	0.03091	0.01411	0.03091
		O	0.83300	0.08401	0.03179	0.08401	0.03179
GOF (χ^2)			1.954 (3)	1.585 (5)		1.694 (1)	

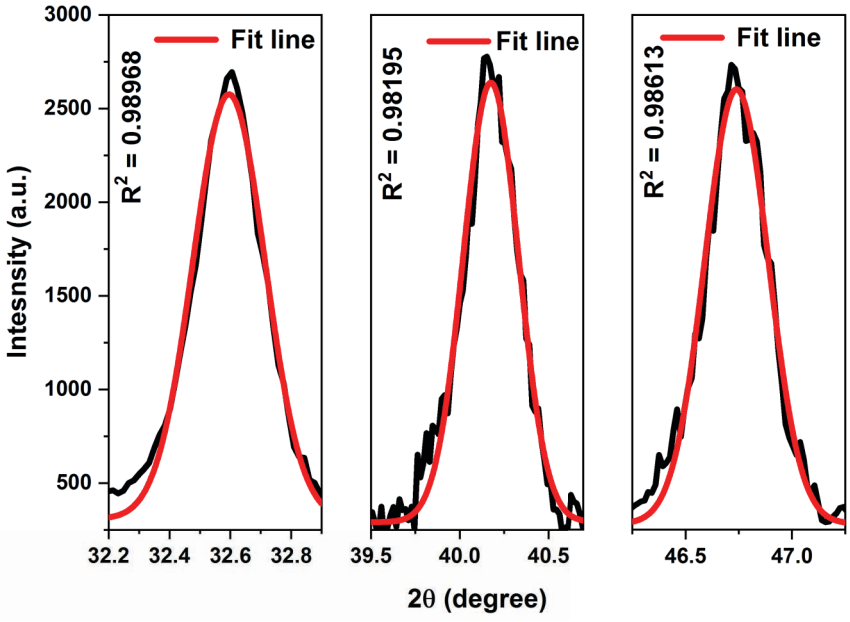

Figure 3: Shows the XRD peaks for 110,111 and 200 peaks fitted to Gaussian function for $(Bi_{0.5}Na_{0.5})TiO_3$ ceramic.

Table 3: Details of the Parameters Used to Calculate the Strain of $((Bi_{(0.4)}Ba_{0.1})Na_{0.5})TiO_3$ Ceramic

Plane	2θ	Sinθ	Cosθ	FWHM $_{obs.}$ (degree)	FWHM $_{inst.}$ (degree)	FWHM $_{tot.}$ (degree)	FWHM $_{tot.}$ (radian)	FWHM$_{tot.}$ cosθ
110	32.59541	0.28063	0.95982	0.27868	0.23669	0.14711	0.00257	0.00246
111	40.1755	0.34346	0.93917	0.36652	0.3113	0.19347	0.00337	0.00317
200	46.7396	0.39666	0.91796	0.35219	0.29913	0.1859	0.00324	0.00298

$FWHM_{obs}$ values of the peaks measured from the fitted peaks are given in Table **3**.

The reflection of the 2θ value of the XRD data is used to compute the average crystalline size of all samples from the Debye Scherrer equation which is as follows [30]

$$t = \frac{k\lambda}{\beta \cos\theta} \quad (1)$$

Where, t is the average crystallite size, k = 0.89 is the Scherrer constant, λ =1.5406 Å is the wavelength of the X-ray beam and β is the full-width half. However, the Scherrer formula does not give an accurate size because it does not account for the lattice strain.

Thus, to calculate the accurate crystallite size Williamson's-Hall plots was constructed as shown in Figure **4a-c** for $((Bi_{(0.5-x)}Ba_x)Na_{0.5})TiO_3$ (where $0.00 \leq x \leq 0.30$) ceramics. The Williamsons hall is used for deconvoluting shapes (crystalline shapes) and strain that contributes to X-ray line broadening because Scherrer's formula does not take the strain contribution into the account.

The small crystallite size (β_{size}) and the broadening caused by the lattice strain (β_{strain}) together gives the X-ray line broadening (β) in the sample i.e. [30-32]

Total broadening = Broadening due to crystallite size + Broadening due to strain

$$\beta = \beta_{size} + \beta_{strain} \quad (2)$$

Where, β_{size} again the Debye Scherrer equation:

$$\beta_{size} = \frac{k\lambda}{t \cos\theta} \quad (3)$$

And also,

$$\beta_{strain} = 4\eta \tan\theta \quad (4)$$

Here, η = Δl/l is the strain and θ is the peak position in radians.

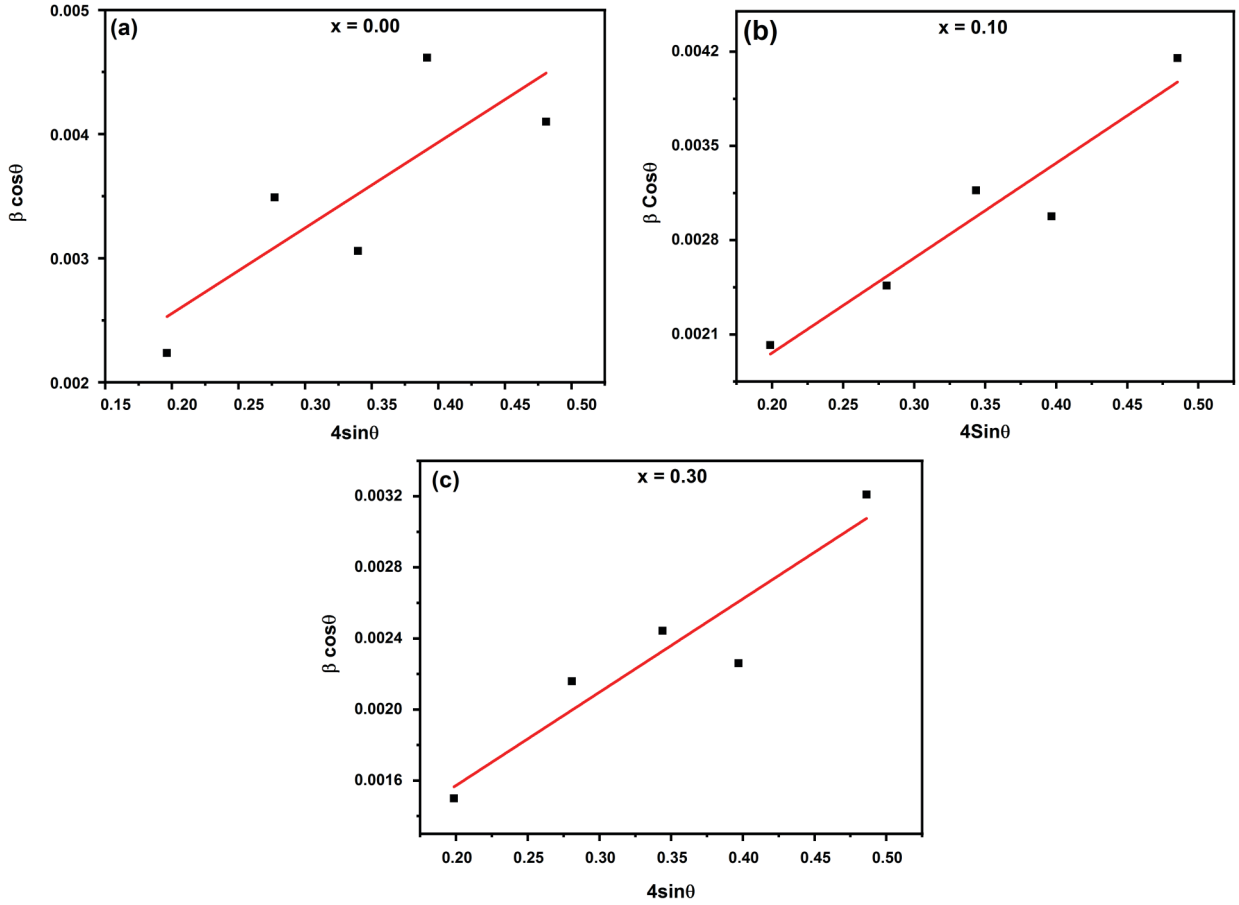

Figure 4: (**a-c**) Willam-Hall plots for $((Bi_{(0.5-x)}Ba_x)Na_{0.5})TiO_3$ at x = 0.00, 0.10, and 0.30 ceramics.

So, putting the values of β_{size} and β_{strain} in equation 1, we get,

$$\beta = \frac{k\lambda}{t\cos\theta} + 4\eta\tan\theta \quad (5)$$

As we know,

$$\tan\theta = \frac{\sin\theta}{\cos\theta}$$

Therefore, equation (5) can be written as,

$$\beta = \frac{k\lambda}{t\cos\theta} + 4\eta\frac{\sin\theta}{\cos\theta}$$

Multiplying both sides by cosθ we get:

$$\beta\cos\theta = \frac{k\lambda}{t} + 4\eta\sin\theta$$

Or

$$\beta\cos\theta = \eta(4\sin\theta) + \frac{k\lambda}{t} \quad (6)$$

The equation represents a straight line, in which η is the gradient (slope) of the line and $\frac{k\lambda}{t}$ is the y-intercept.

Consider the standard equation of a straight line,

$$y = mx + c \quad (7)$$

Now, we will plot 4 sinθ on the x-axis and $\beta\cos\theta$ on the y-axis.

The value of the strain (η) will be given by the value of "m" which represents the gradient (slope) of the line and the crystallite size can be calculated from the y-intercept $\frac{k\lambda}{t}$.

The average crystallite size of ceramics decreases (i.e. 63.59 to 30.11 nm) and strain increases from 5.25 × 10^{-3} to 7.74 × 10^{-3} as the Ba^{2+} content increases in the BBNT ceramics, respectively (as given in Table **4**). The substitution of Ba^{2+} (1.39 Å) for the smaller ionic radii of Bi^{3+} (~1.17 Å), causes the lattice distortion. Thus, the increase in Ba^{2+} content results in an increase in the

Table 4: Crystal and Dielectric Parameters of $((Bi_{(0.5-x)}Ba_x)Na_{0.5})TiO_3$ Ceramics

Composition		*x* = 0.00	*x* = 0.10	*x* = 0.30
Crystallite Size (nm)	W-H Plots	65.83	50.68	32.05
	Scherrer Formula	63.59	49.73	30.11
Crystallite strain		5.25×10^{-3}	7.05×10^{-3}	7.74×10^{-3}
Transition temperature	T_1 (°C)	80	90	-------
	T_C (°C)	250	280	300
Dielectric constant (ε)		2917	2698	5563

lattice strain, which further results in the reduction of crystallite size of these ceramics.

3.2. Scanning Electron Microscope (SEM)

Figure **5a** and **b** for *x* = 0.00, (c and d) for *x* = 0.10, and (e and f) for *x* = 0.30) represents the SEM images of $((Bi_{(0.5-x)}Ba_x)Na_{0.5})TiO_3$ ceramics. It was observed that the average grain size increases with an increase in Ba concentration [33]. Small crystallites are leading information of larger size grains (as results of small crystallites obtained in XRD section) may be another reason for larger size grains. The BNT with *x* = 0.00 and 0.10 samples are more compact and exhibited

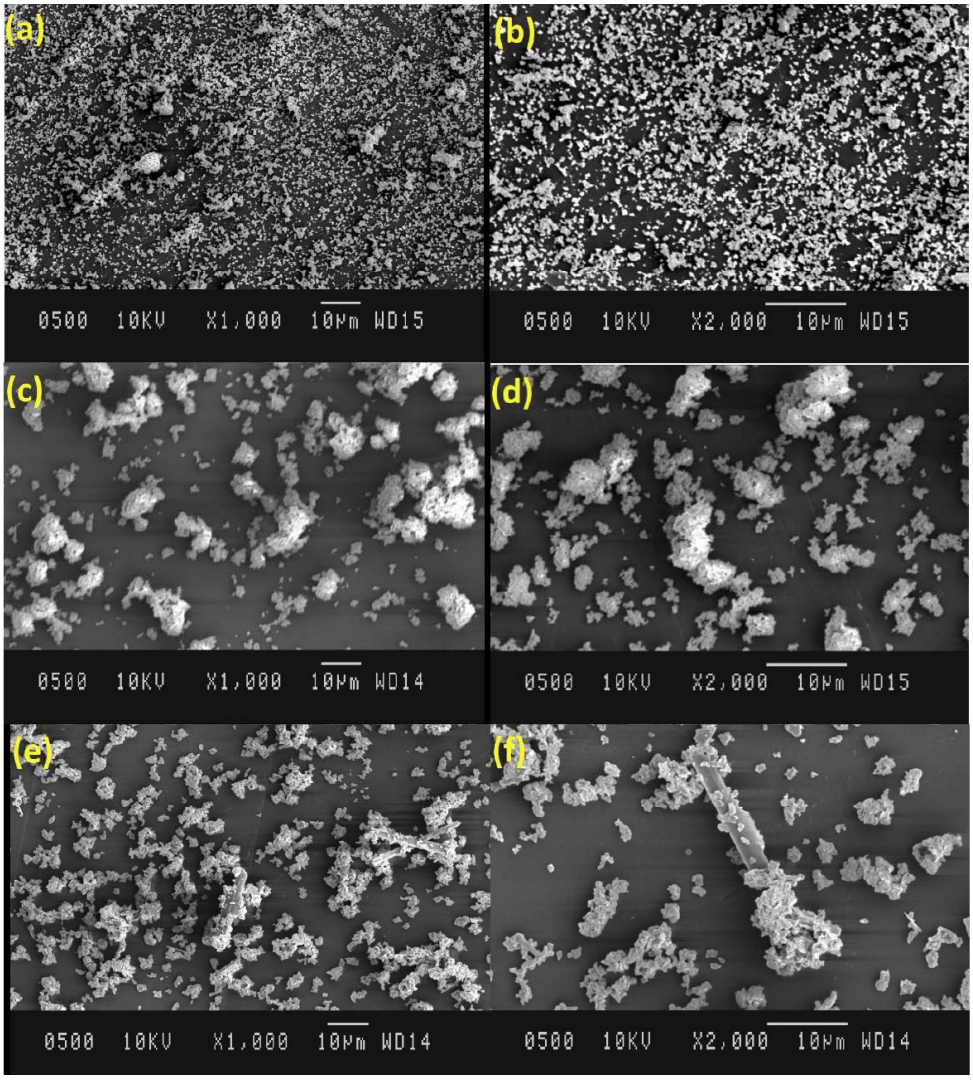

Figure 5: SEM images of $((Bi_{(0.5-x)}Ba_x)Na_{0.5})TiO_3$ ((**a** and **b**) for *x* = 0.00, (**c** and **d**) for *x* = 0.10 and (**e** and **f**) for *x* = 0.30) ceramics.

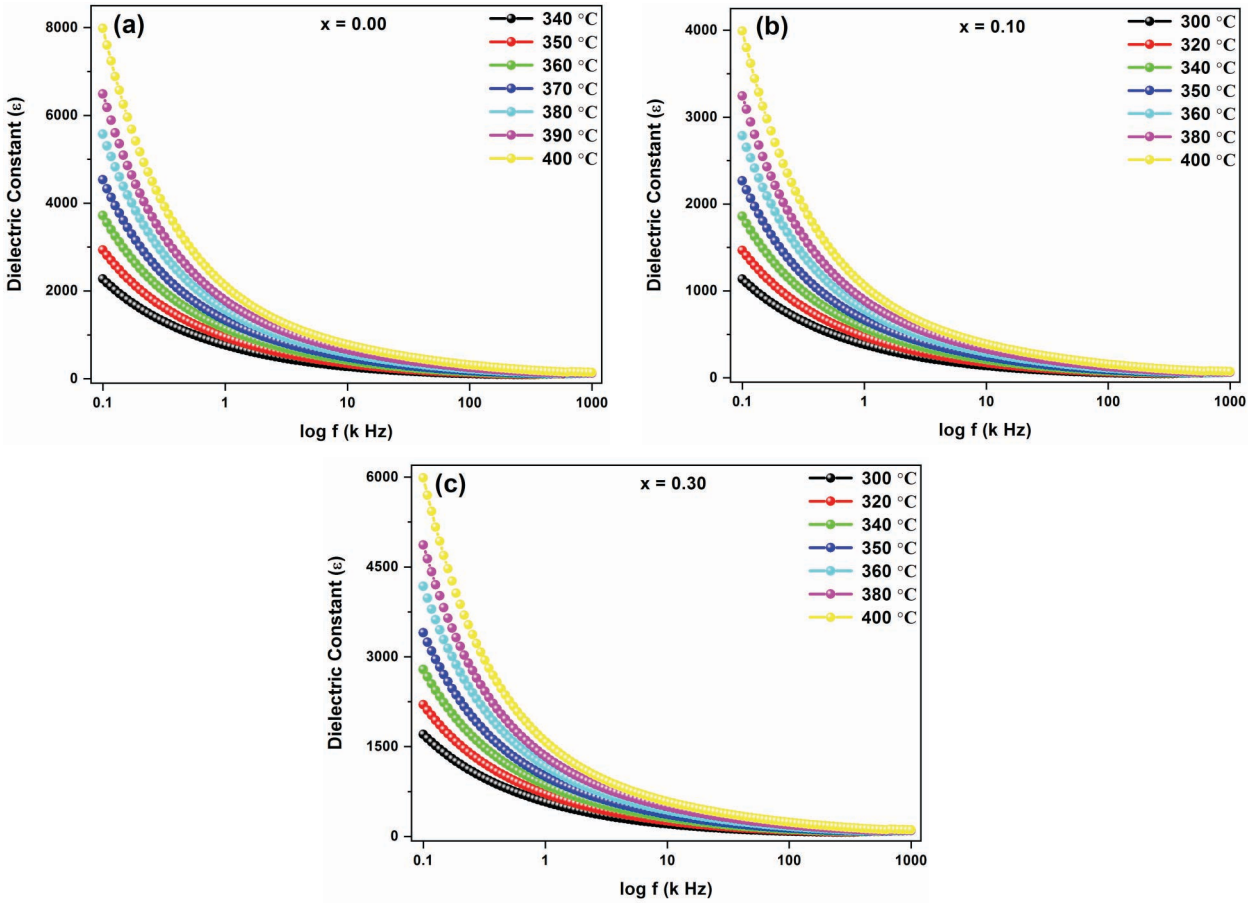

Figure 6: (**a-c**) Frequency dependent dielectric behavior of $((Bi_{(0.5-x)}Ba_x)Na_{0.5})TiO_3$ for x = 0.00, 0.10 and 0.30 ceramics.

uniform microstructure with smaller grains, due to the formation of MPB [34].

3.3. Dielectric Studies

Figure **6a-c** shows the variation of Dielectric constant (ε) as a function of frequency of $((Bi_{(0.5-x)}Ba_x)Na_{0.5})TiO_3$ (where $0.00 \leq x \leq 0.30$) ceramics at higher temperature (i.e. 300 to 400 °C). It is observed from these figures that there is a decrease in the value of the dielectric constant with an increase in frequency, which is a typical characteristic of normal dielectric [35].

A high dielectric constant at low frequencies is characteristic of all-dielectric materials, which means overall polarization contributes to the dielectric constant. With an increase in frequency the dielectric constant decrease due to the frequency-dependent nature of polarization. The order of different polarization is ionic < dipolar < atomic < electronic shows dominance up to frequency 10^7, 10^{11}, 10^{15} Hz, and electronic polarization shows its dominance even in G Hz or above range [36]. This means different polarization vanishes with the increase in the frequency and thus leading to a decrease in the value of the dielectric constant. Thus, the value of the dielectric constant decreases at high frequency.

Temperature dependence of Dielectric constant (ε) for $((Bi_{(0.5-x)}Ba_x)Na_{0.5})TiO_3$ (where $0.00 \leq x \leq 0.30$) Ceramics (at frequencies 1, 10, 100 k Hz and 1 M Hz) is shown in Figure **7a-c**, respectively. From these figures, two phenomena were observed. They were; (i) In ceramics x = 0.00 and 0.10 two peaks were observed, the first peak corresponds to ferroelectric-ferroelectric (ε_1) and the second peak corresponds to ferroelectric-paraelectric phase transitions (ε_2). The first phase transition shows a structural change from rhombohedral to tetragonal and the second phase transition from tetragonal to the cubic structure. The first phase transition is well supported by XRD as getting rhombohedral structure at room temperature. With a further increase in Ba content (i.e. at x = 0.30), the value of the dielectric constant gradually increased to (5563) at 1 k Hz, and T_C shifted to 300 °C. (ii) The decrease in the value dielectric constant with increase in frequency because of frequency-dependent nature. The various values of dielectric constant and phase transition temperatures are shown in Table **4**.

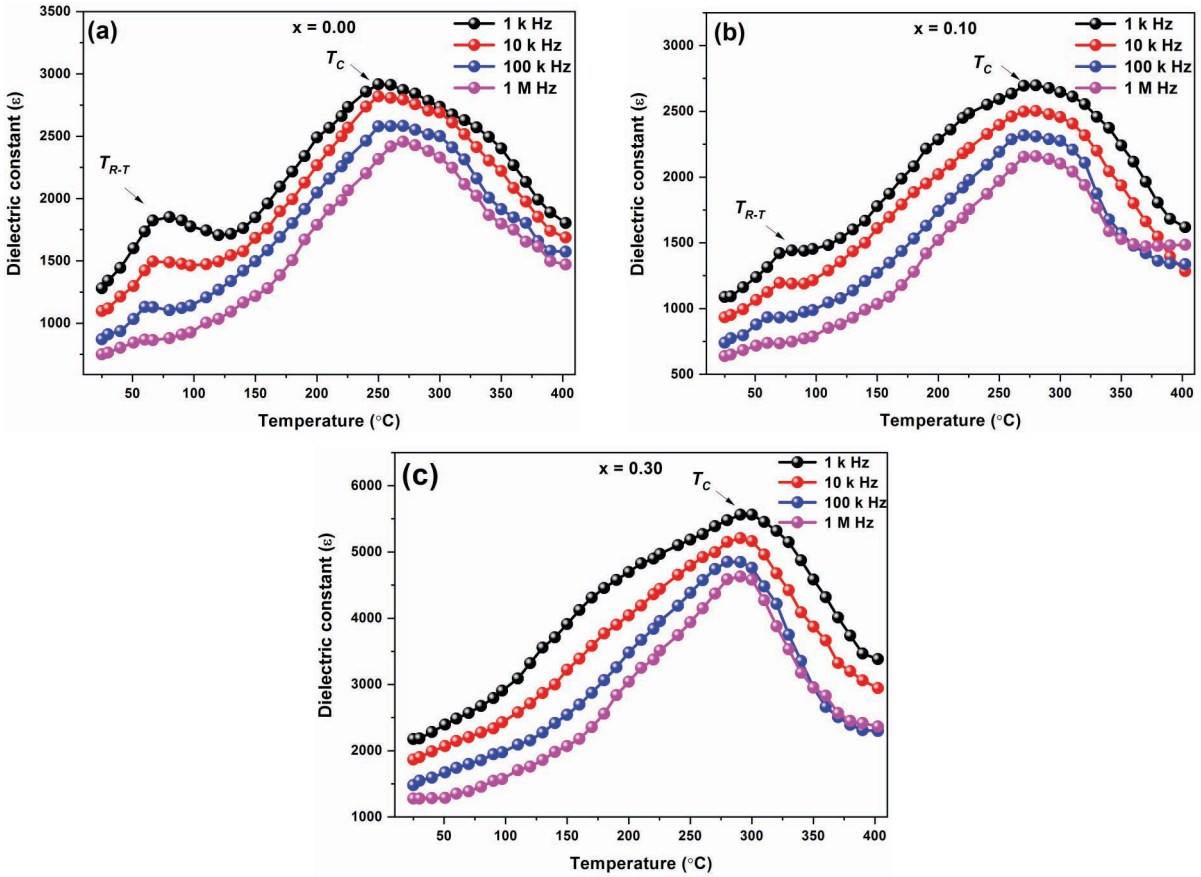

Figure 7: (**a-c**) Temperature dependent dielectric behavior of $((Bi_{(0.5-x)}Ba_x)Na_{0.5})TiO_3$ for x = 0.00, 0.10 and 0.30 ceramics.

The ac conductivity in ceramics is mainly controlled by the migration of space charges under the action of the electric field and by the defect-ion complexes, the polarization field, the relaxation, etc. The ac conductivity of ceramics was calculated using the formula:

$$\sigma_{ac} = 2\pi f \varepsilon_0 \varepsilon \tan(\delta) \quad (8)$$

Where f is the applied frequency in Hz,

ε_0 = Permittivity of the free space = 8.85* 10^{-12} Fm^{-1}, ε = Permittivity of ceramics and tan δ = loss tangent

Figure **8a-c** represents the ac conductivity of $((Bi_{(0.5-x)}Ba_x)Na_{0.5})TiO_3$ (where $0.00 \leq x \leq 0.30$) ceramic as a function of frequency in the high temperature range (i.e. 300 to 400 °C). The σ (f) curves are found to be merging at high frequency due to the presence of more defect mobility and high conductivity in the materials [37]. The magnitude of ac conductivity increases with an increase in temperature. Because the band-gap decreases with an increase in temperature and ions in the valance band get thermal energy (in form of heat) easily jump to conduction and resulting in high conductivity. The increase in conductivity on doping is due to an increase in the specific surface area in x = 0.30 ceramic.

4. CONCLUSION

Ba-doped BNT lead-free ceramics were synthesized successfully by the conventional solid-state reaction method. Rietveld's refinement of the XRD pattern confirms the structural change from rhombohedral to tetragonal with MPB. W-H plots show that crystallite size increases with a decrease in lattice strain. SEM shows that an increase in grain size was recorded with the increase in Ba-doping. The dielectric constant of BBNT ceramics is increased with the addition of Ba-content. An increase in the ac conductivity was observed on doping which is due to an increase in the specific surface area.

5. FUTURE DEVELOPMENT AND RESEARCH PROPOSED

- Extension of this work is suggested towards HRTEM for confirming the particle size and structure.

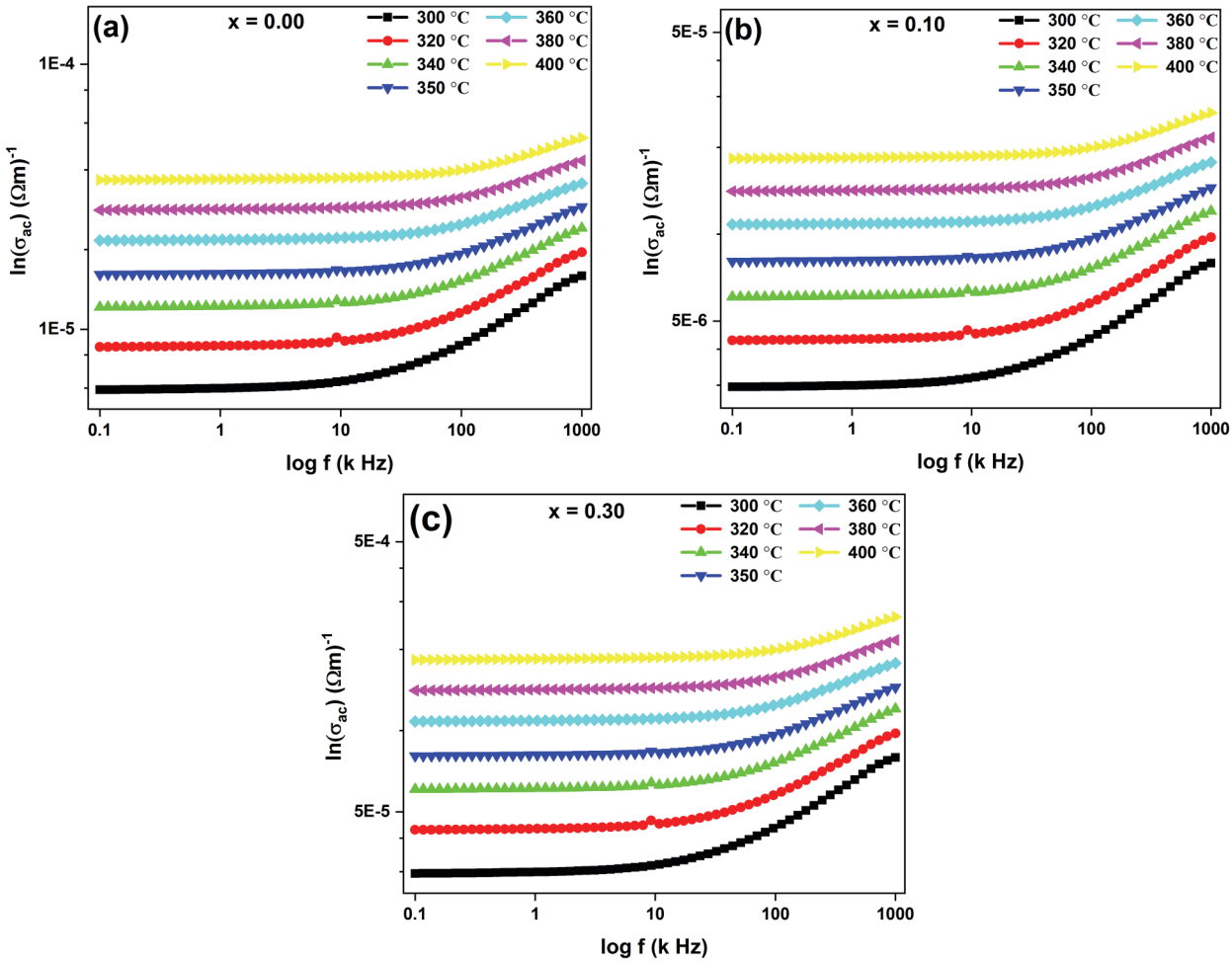

Figure 8: (**a-c**) Frequency dependent ac conductivity behavior of $((Bi_{(0.5-x)}Ba_x)Na_{0.5})TiO_3$ for x = 0.00, 0.10 and 0.30 ceramics.

- XPS/EDAX for confirming the presence of different elements within the ceramics.
- FESEM of sintered ceramics to check the grain, grain boundary formation and can be able to an established relationship between structural and electrical properties of materials.

REFERENCES

[1] Liu X, Yin J, Wu J. A new class of ion substitution to achieve high electrostrain under low electric field in BNT‐based ceramics. Journal of the American Ceramic Society 2021. https://doi.org/10.1111/jace.18008

[2] Zheng T, *et al*. The structural origin of enhanced piezoelectric performance and stability in lead free ceramics. Energy & Environmental Science 2017; 10(2): 528-537. https://doi.org/10.1039/C6EE03597C

[3] Somlenski G, Agramovaskaya A. Dielectric polarization of a number of complex compounds. Sov Phys Solid State 1960; 1(10): 1429-1437.

[4] Dai YJ, Pan JS, Zhang XW. Composition range of morphotropic phase boundary and electrical properties of NBT-BT system in Key Engineering Materials. Trans Tech Publ 2007. https://doi.org/10.4028/0-87849-410-3.206

[5] Yang Z, *et al*. Structure and electrical properties of (1− x) Bi0. 5Na0. 5TiO3–xBi0. 5K0. 5TiO3 ceramics near morphotropic phase boundary. Materials Research Bulletin 2008; 43(1): 81-89. https://doi.org/10.1016/j.materresbull.2007.02.016

[6] Wang X, Chan HLW, Choy CL. (Bi1/2Na1/2) TiO3–Ba (Cu1/2W1/2) O3 Lead‐Free Piezoelectric Ceramics. Journal of the American Ceramic Society 2003; 86(10): 1809-1811. https://doi.org/10.1111/j.1151-2916.2003.tb03562.x

[7] Yan F, *et al*. Significantly enhanced energy storage density and efficiency of BNT-based perovskite ceramics via A-site defect engineering. Energy Storage Materials 2020; 30: 392-400. https://doi.org/10.1016/j.ensm.2020.05.026

[8] Yoneda Y, Noguchi Y. Nanoscale structural analysis of Bi0. 5Na0. 5TiO3. Japanese Journal of Applied Physics 2020; 59(SP): SPPA01. https://doi.org/10.35848/1347-4065/aba2c2

[9] Suchanicz J, *et al*. Dielectric and structural relaxation phenomena in Na0. 5Bi0. 5TiO3 single crystal. Phase Transitions: A Multinational Journal 1996; 57(4): 173-182. https://doi.org/10.1080/01411599608208744

[10] Shi J, *et al*. Bi deficiencies induced high permittivity in lead-free BNBT–BST high-temperature dielectrics. Journal of Alloys and Compounds 2015; 627: 463-467. https://doi.org/10.1016/j.jallcom.2014.12.022

[11] Yu Y, *et al*. Room temperature ferroelectricity in donor-acceptor co-doped TiO2 ceramics using doping-engineering. Acta Materialia 2018; 150: 173-181. https://doi.org/10.1016/j.actamat.2018.03.016

[12] Dittmer R, *et al*. A High-Temperature-Capacitor Dielectric Based on K 0.5 Na 0.5 NbO 3-Modified Bi 1/2 Na 1/2 TiO 3–Bi 1/2 K 1/2 TiO 3. Journal of the American Ceramic Society 2012; 95(11): 3519-3524. https://doi.org/10.1111/j.1551-2916.2012.05321.x

[13] Li M, *et al*. Donor-doping and reduced leakage current in Nb-doped Na0. 5Bi0. 5TiO3. Applied Physics Letters 2015; 106(10): 102904. https://doi.org/10.1063/1.4914509

[14] Yang F, *et al*. Defect chemistry and electrical properties of sodium bismuth titanate perovskite. Journal of Materials Chemistry A 2018; 6(13): 5243-5254. https://doi.org/10.1039/C7TA09245H

[15] Takenaka T, Nagata H. Current status and prospects of lead-free piezoelectric ceramics. Journal of the European Ceramic Society 2005; 25(12): 2693-2700. https://doi.org/10.1016/j.jeurceramsoc.2005.03.125

[16] Li M, *et al*. A family of oxide ion conductors based on the ferroelectric perovskite Na 0.5 Bi 0.5 TiO 3. Nature Materials 2014; 13(1): 31-35. https://doi.org/10.1038/nmat3782

[17] Zheng T, *et al*. Recent development in lead-free perovskite piezoelectric bulk materials. Progress in Materials Science 2018; 98: 552-624. https://doi.org/10.1016/j.pmatsci.2018.06.002

[18] Hong Y-H, *et al*. High electromechanical strain properties by the existence of nonergodicity in LiNbO3–modified Bi1/2Na1/2TiO3–SrTiO3 relaxor ceramics. Ceramics International 2018; 44(17): 21138-21144. https://doi.org/10.1016/j.ceramint.2018.08.156

[19] Xie H, *et al*. Structure, dielectric, ferroelectric, and field-induced strain response properties of (Mg1/3Nb2/3) 4+ complex-ion modified Bi0. 5 (Na0. 82K0. 18) 0.5 TiO3 lead-free ceramics. Journal of Alloys and Compounds 2018; 743: 73-82. https://doi.org/10.1016/j.jallcom.2018.01.367

[20] Yan B, *et al*. Giant electro-strain and enhanced energy storage performance of (Y0. 5Ta0. 5) 4+ co-doped 0.94 (Bi0. 5Na0. 5) TiO3-0.06 BaTiO3 lead-free ceramics. Ceramics International 2020; 46(1): 281-288. https://doi.org/10.1016/j.ceramint.2019.08.261

[21] Takenaka T, Okuda T, Takegahara K. Lead-free piezoelectric ceramics based on (Bi1/2Na1/2) TiO3-NaNbO3. Ferroelectrics 1997; 196(1): 175-178. https://doi.org/10.1080/00150199708224156

[22] Fu P, *et al*. Effect of Dy2O3 on the structure and electrical properties of (Bi0. 5Na0. 5) 0.94 Ba0. 06TiO3 lead-free piezoelectric ceramics. Journal of Alloys and Compounds 2010; 508(2): 546-553. https://doi.org/10.1016/j.jallcom.2010.08.117

[23] Rawat M, *et al*. Structural, dielectric and conductivity properties of Ba2+ doped (Bi0. 5Na0. 5) TiO3 ceramic. Advanced Materials Letters 2012; 3(4): 286-292. https://doi.org/10.5185/amlett.2012.2322

[24] Lin Y, *et al*. Effects of doping Eu2O3 on the phase transformation and piezoelectric properties of Na0. 5Bi0. 5TiO3-based ceramics. Materials Science and Engineering: B 2003; 99(1-3): 449-452. https://doi.org/10.1016/S0921-5107(02)00465-8

[25] Herabut A, Safari A. Processing and electromechanical properties of (Bi0. 5Na0. 5)(1− 1.5 x) LaxTiO3 ceramics. Journal of the American Ceramic Society 1997; 80(11): 2954-2958. https://doi.org/10.1111/j.1151-2916.1997.tb03219.x

[26] Lee J-K, *et al*. Phase transitions and dielectric properties in A-site ion substituted (Na 1/2 Bi 1/2) TiO 3 ceramics (A= Pb and Sr). J Appl Phys 2002; 91(7): 4538-4542. https://doi.org/10.1063/1.1435415

[27] Nagata H, *et al*. Correlation between depolarization temperature and lattice distortion in quenched (Bi 1/2 Na 1/2) TiO 3-based ceramics. Appl Phys Express 2020. https://doi.org/10.35848/1882-0786/ab8c1d

[28] Guerra J, *et al*. Room temperature antiferroelectric-phase stability in BNT-BT lead-free ceramics. Physica B: Condensed Matter 2017; 525: 114-118. https://doi.org/10.1016/j.physb.2017.09.014

[29] Lal M, *et al*. Structural, Dielectric and Impedance Studies of KNNS–BKT Ceramics. Am J Mater Sci 2017; 7(2): 25-34.

[30] Suryanarayana C, Norton MG. X-ray diffraction: a practical approach. Springer Science & Business Media 2013.

[31] Pal V, Dwivedi R, Thakur O. Synthesis and ferroelectric behavior of Gd doped BNT ceramics. Curr Appl Phys 2014; 14(1): 99-107. https://doi.org/10.1016/j.cap.2013.10.007

[32] Goel P, Yadav K. Substitution site effect on structural and dielectric properties of La–Bi modified PZT. J Mater Sci 2007; 42(11): 3928-3935. https://doi.org/10.1007/s10853-006-0416-x

[33] Yang C, *et al*. Effect of Ba doping on magnetic and dielectric properties of nanocrystalline BiFeO3 at room temperature. Journal of Alloys and Compounds 2010; 507(1): 29-32. https://doi.org/10.1016/j.jallcom.2010.07.193

[34] Pattipaka S, Bora S, Pamu D. Structural, Electrical, and AC-Resistivity Studies of BNT-KN Piezoelectric Ceramics. Ferroelectrics 2020; 557(1): 28-42. https://doi.org/10.1080/00150193.2020.1713360

[35] Kumar P, Kar M. Effect of structural transition on magnetic and optical properties of Ca and Ti co-substituted BiFeO3 ceramics. Journal of Alloys and Compounds 2014; 584: 566-572. https://doi.org/10.1016/j.jallcom.2013.09.107

[36] Mehrotra P, Chatterjee B, Sen S. EM-wave biosensors: A review of RF, microwave, mm-wave and optical sensing. Sensors 2019; 19(5): 1013. https://doi.org/10.3390/s19051013

[37] Zhu C, *et al*. High temperature lead-free BNT-based ceramics with stable energy storage and dielectric properties. J Mater Chem A 2020; 8(2): 683-692. https://doi.org/10.1039/C9TA10347C